



3 4456 0278874 9

ORNL/TM-10030

ornl

OAK RIDGE
NATIONAL
LABORATORY

MARTIN MARIETTA

Compact Torsatron Configurations

B. A. Carreras
N. Dominguez
L. Garcia
V. E. Lynch
J. F. Lyon
J. R. Cary
J. D. Hanson
A. P. Navarro

OAK RIDGE NATIONAL LABORATORY
CENTRAL RESEARCH LIBRARY
CIRCULATION SECTION
4009 ROOM 125
LIBRARY LOAN COPY
DO NOT TRANSFER TO ANOTHER PERSON
If you wish someone else to see this
report, send in some with report and
the library will arrange a loan.

Printed in the United States of America. Available from
National Technical Information Service
U.S. Department of Commerce
5285 Port Royal Road, Springfield, Virginia 22161
NTIS price codes—Printed Copy: A03; Microfiche A01

This report was prepared as an account of work sponsored by an agency of the United States Government. Neither the United States Government nor any agency thereof, nor any of their employees, makes any warranty, express or implied, or assumes any legal liability or responsibility for the accuracy, completeness, or usefulness of any information, apparatus, product, or process disclosed, or represents that its use would not infringe privately owned rights. Reference herein to any specific commercial product, process, or service by trade name, trademark, manufacturer, or otherwise, does not necessarily constitute or imply its endorsement, recommendation, or favoring by the United States Government or any agency thereof. The views and opinions of authors expressed herein do not necessarily state or reflect those of the United States Government or any agency thereof.

ORNL/TM-10030
Dist. Category UC-20 g

Fusion Energy Division

COMPACT TORSATRON CONFIGURATIONS

B. A. CARRERAS
N. DOMINGUEZ
L. GARCIA
V. E. LYNCH
J. F. LYON
J. R. CARY^a
J. D. HANSON^b
A. P. NAVARRO^c

^aUniversity of Colorado, Boulder, CO 80304

^bAuburn University, Auburn, AL 36848

^cAsociacion EURATOM/CIEMAT, Madrid, Spain

DATE PUBLISHED — September 1987

Prepared by the
OAK RIDGE NATIONAL LABORATORY
Oak Ridge, Tennessee 37831
operated by
MARTIN MARIETTA ENERGY SYSTEMS, INC.
for the
U.S. DEPARTMENT OF ENERGY
under contract DE-AC05-84OR21400

MARTIN MARIETTA ENERGY SYSTEMS LIBRARIES



3 4456 0278874 9

CONTENTS

ABSTRACT	v
1. INTRODUCTION	1
2. VACUUM MAGNETIC FIELD PROPERTIES OF LOW-ASPECT-RATIO TORSATRONS	3
3. VACUUM MAGNETIC FIELD OPTIMIZATION OF LOW-ASPECT-RATIO TORSATRONS	6
4. MHD PROPERTIES OF THE COMPACT TORSATRON CONFIGURATIONS	8
5. FRAGILITY OF THE MAGNETIC SURFACES FOR COMPACT TORSATRON CONFIGURATIONS	10
6. CONCLUSIONS	12
REFERENCES	13

ABSTRACT

Low-aspect-ratio stellarator configurations can be realized by using torsatron winding. Plasmas with aspect ratios in the range of 3.5 to 5 can be confined by these Compact Torsatron configurations. Stable operation at high β should be possible in these devices, if a vertical field coil system is adequately designed to avoid breaking of the magnetic surfaces at finite β .

1 INTRODUCTION

Stellarators have traditionally been considered large-aspect-ratio configurations. In recent years, however, interest in low-aspect-ratio stellarators has increased [1,2]. Many configurations are being studied, and some of the experiments being proposed have a plasma aspect ratio, $A_p = R/\bar{a}$, below 10. The Advanced Toroidal Facility (ATF) [1], ready to begin operation at Oak Ridge National Laboratory (ORNL), has 12 toroidal field periods and a plasma aspect ratio of 7.5. The CHS device [2], under construction at Nagoya University, has eight toroidal field periods and a plasma aspect ratio of 5. A motivating factor for studies of low-aspect-ratio stellarators is the move toward a more compact stellarator, which could make a more attractive fusion reactor [3,4]. Another factor which is important for present-day experiments is to have larger plasmas for a given-size device. Critical physics issues for low-aspect-ratio stellarators are the potential for (1) low-equilibrium β limit, (2) fragility of the magnetic surfaces, and (3) unfavorable scaling of the neoclassical transport coefficients with aspect ratio. These three critical issues were discussed in a general sense in Ref. 6. This paper focuses on the first two.

A low-equilibrium β limit is correlated with a low rotational transform at the plasma edge, which is proportional to the aspect ratio for configurations with the same helical coil pitch. Fragility of magnetic surfaces is a result of the lack of symmetry of the system because of the mixing of toroidal and helical effects, which becomes more important with low-aspect-ratio configurations. Symmetry breaking increases with β , and, thus, so does the likelihood of breaking the outer magnetic surfaces. For low-aspect-ratio configurations, the breaking of magnetic surfaces can be the dominant cause of limiting the equilibrium β . Even if that is not case, breaking of the outer magnetic surfaces can contribute to lowering the equilibrium β limit by further reducing of the edge transform.

The conventional wisdom states that the equilibrium β limit for a stellarator scales as $\beta_c \approx \frac{\tau_a^2}{A_p}$. Here, τ_a is the rotational transform at the plasma edge, and the equilibrium β critical, β_c , has been defined as the value of β for which the toroidally averaged magnetic axis shift, Δ , is half the average minor radius, \bar{a} . Because the edge rotational transform scales as the aspect ratio, this β_c scaling indicates a reduction of the equilibrium β limit with decreasing aspect ratio. However, the reduction is not as bad as this simple scaling indicates because the nonlinear increase of Δ with β is less than this lowest-order result, as shown in Ref. 6. In addition, increasing the edge rotational transform opens a path for increasing β_c . In carrying out low-aspect-ratio configuration studies, the rotational transform can be increased in several ways by modifying the helical coil system. As shown in this paper, the problem can be approached by starting from a standard helical coil and varying the pitch, the cross-sectional shape of the winding surface, and the winding law of the helical coils. An alternative approach to improve the equilibrium β limit, based on the minimization of Pfirsch-Schlüter currents, has been taken by the Wendelstein group [5]. However, up to now this optimization approach has been applied only to large-aspect-ratio stellarator configurations. In contrast, the current study is concerned with torsatron configurations with aspect ratios below 5 and toroidal field periods, M , in the range of 6 to 9.

An important issue in our approach is to find an efficient method of handling the large number of degrees of freedom involved in the process. Such a method, developed by Cary and Hanson [6], is based on the equivalence of toroidal magnetic fields to a Hamiltonian system. The method, which aims at elimination of magnetic field line stochasticity, has been applied to the sequence of low- M ($M = 9$ to 6) torsatron configurations. As a result, a sequence of configurations with decreasing aspect ratio but with a constant edge rotational transform

just below 1 has been obtained. By using numerical techniques that assume the existence of magnetic surfaces for nonzero β , it can be shown that these configurations have favorable magnetohydrodynamic (MHD) properties. The equilibrium β limit is higher for these configurations than for the unoptimized cases, and it scales as $1/M$. These configurations are stable to 3-D ideal Mercier modes. By using the stellarator expansion [7] technique, it is possible to show that they are also stable to low- n modes.

For nonzero β values, the main question concerning the viability of these configurations is still the fragility of the magnetic surfaces. Indeed, as β increases and the plasma shifts outward, changes in the magnetic field spectrum can destroy the results of the vacuum field optimization. A practical way of resolving this problem is to do the magnetic surface optimization for the vacuum magnetic field by varying the currents in four pairs of axisymmetric vertical field (VF) coils. Similar optimized configurations are obtained in this way. This has two consequences. First, the problem of accurately constructing a helical coil is not overly demanding because the VF coil system can be used to correct for winding law errors. Second, it gives a way of compensating for β effects on the magnetic surfaces. This offers a potential solution to the problem of fragility of magnetic surfaces for small-aspect-ratio configurations.

2 VACUUM MAGNETIC FIELD PROPERTIES OF LOW-ASPECT-RATIO TORSATRONS

The starting point for the vacuum magnetic field calculations is a set of realistic coils. For an $\ell = 2$ torsatron, the coil configuration consists of two helical conductors, carrying current in the same direction and wound on a torus of major radius R_c . The coil position is given by

$$R = R_c + a_1 \cos \theta + a_2 \cos 2\theta \quad (1)$$

$$Z = e(a_1 \sin \theta - a_2 \sin 2\theta) \quad (2)$$

where R and Z are the usual cylindrical coordinates for a toroidal configuration and the winding law is defined by

$$\phi = \phi_0 + \ell \left[\theta - \sum \alpha_n \sin(n\theta) \right] / M \quad (3)$$

Here ϕ and θ are the toroidal and poloidal angles, respectively. An average minor radius of the coil, \bar{a}_c , can be defined as the square root of the area of the winding cross section of the torus divided by π , which gives $\bar{a}_c = \sqrt{a_1^2 - 2a_2^2}$. If $a_2 = 0$ in Eqs. (1) and (2), the winding cross section of the torus is circular and the coil radius is $\bar{a}_c = a_1$. The parameter e in Eq. (2) is the ellipticity, which for most calculations in this paper is $e = 1$. In addition, an external vertical magnetic field must be provided to define the location of the magnetic axis and to allow formation of closed magnetic surfaces. The VF coil system consists, in general, of several pairs of axisymmetric coils. The dipole and quadrupole moments of this coil system can be used to control some physics parameters of the configuration [8].

The main helical coil parameters varied in these studies are the coil aspect ratio $A_c = R_c/\bar{a}_c$, the number of field periods M , the helical coil pitch parameter $p_c = M/(\ell A_c)$, the triangularity of the torus winding cross section $\delta_T = \frac{-6a_2}{a_1 + \sqrt{a_1^2 + 32a_2^2}}$, and the winding law parameters, α_n . By changing these parameters, the main physics characteristics of the vacuum configuration (namely, rotational transform ι , shear, well depth, and shape of the vacuum flux surfaces) can be varied.

The studies presented here used the same techniques as those in Ref. 11. In that paper, the configurations studied had basically $M > 10$ and plasma aspect ratios, A_p , above 5. Here we focus our attention on configurations with $M < 10$. The objective is to find low-aspect-ratio configurations, $A_p < 5$, with good flux surfaces and physics properties similar to those of the $M = 12$ configuration in Ref. 11, on which the ATF device is based [1]. The results presented here are for a fixed-coil major radius, which for convenience is taken to be $R_c = 1$ m. All other lengths are given in meters.

To show the dependence of the properties of the magnetic configuration on the p_c and M parameters, we have calculated a sequence of magnetic configurations by varying M between 6 and 9 and p_c between from 1.3 and 1.5. The magnetic surfaces for this sequence at the beginning of a field period have been plotted in Fig. 1. Let us consider the main properties of this configuration. For a fixed-coil pitch, decreasing the number of field periods decreases the aspect ratio, rotational transform, and shear (Fig. 2a). If the rotational transform becomes zero at a radial point, an internal separatrix forms (i.e., the magnetic axis bifurcates and an internal X-point may form for low values of M). This is shown in Fig. 1 for the configuration scan with fixed pitch, $p_c = 1.4$. In this sequence, the $M = 6$ configuration has a magnetic surface topology with multiple magnetic axes. The same happens to higher M

configurations if the helical coil pitch is increased beyond $p_c = 1.4$. Therefore, it is important to choose the helical coil pitch so that the transform is greater than zero and thus ensure that there is no internal separatrix. This can be achieved by reducing the pitch of the helical coil (Fig. 2b). However, as the pitch decreases, the average radius of the last closed magnetic surface and the utilization volume are reduced. Furthermore, the resulting increase in rotational transform does not produce an increase in shear (Fig. 2b). Therefore, although the pitch parameter is more important in the determination of the physics properties for low- M configurations than for high- M configurations, it is not sufficient to use only the helical coil pitch as an optimization parameter. Other degrees of freedom of the helical coil system must be used to achieve the shear, rotational transform, and utilization volume desired.

Although the configurations in Fig. 1 have low shear, their stability properties are not necessarily poor. All these configurations have broad magnetic wells. This is shown in Fig. 3, where the magnetic well has been plotted for three configurations with $M = 7$ and different values of helical coil pitch. In this figure, the magnetic well is defined as $[V'(\rho) - V'(0)]/V'(0)$, where $V'(\rho)$ is the derivative with respect to the toroidal flux of the volume enclosed in a magnetic surface with normalized radius $\rho = \bar{r}/\bar{a}$. It is not the stability properties but rather the low equilibrium limit associated with low transform that is the main concern for these configurations.

Let us now consider the effect on the configuration properties of the cross-sectional shape of the torus on which the helical coils are wound. An elliptical shape for this cross section reduces the rotational transform and magnetic well. Therefore, ellipticity is not a useful parameter for improving the equilibrium properties of low-aspect-ratio configurations and has not been used in the present studies. Also, the effect of ellipticity can always be simulated by the quadrupole component of the vertical field.

A triangular shape for the torus winding cross section can have a more interesting effect on the physics parameters of low-aspect-ratio torsatrons. In the parameterization of the helical coils [Eqs (1) and (2)], the cross section triangularity is controlled by the parameter a_2 . Depending on the sign of a_2 , the vertex of the triangle points inward ($a_2 < 0$, positive triangularity) or outward ($a_2 > 0$, negative triangularity). As an example, Fig. 4 shows a coil system with the vertex of the triangle pointing inward. This corresponds to an $M = 9$ torsatron configuration with $a_2 = -0.1$. The triangularity of the torus winding cross section has an impact on the physics parameters, as illustrated in Fig. 5 in which the rotational transform and the magnetic well have been plotted for an $M = 8$ torsatron with $p_c = 1.38$. For either sign of a_2 (and hence triangularity), the rotational transform increases as the magnitude of the triangularity increases (Fig. 5a). However, the magnetic well decreases and can even change to a magnetic hill as the triangularity increases. This is demonstrated in Fig. 5b, which plots the magnetic well at the $\epsilon = 0.5$ surface vs triangularity. The effect of the triangularity is stronger for $a_2 > 0$ (negative triangularity), where the shear also increases with the triangularity. Lowering the aspect ratio deepens the magnetic well; increasing the triangularity as the aspect ratio is decreased thus offers a potential trade-off in improving the configuration properties by increasing the rotational transform, shear, and utilization volume. For $M = 8$ and 9 and $A_p \sim 5$, it is possible to find torsatron configurations with physics parameters like those of the ATF configuration by carefully choosing the coil pitch and the triangularity of the torus winding cross section. That is not the case for configurations with a lower number of field periods.

Finally, the other coil parameters to be considered are the winding law parameters, α_n , which also play an important role in the determination of the physics parameters of a

configuration. In the optimization studies described in Section 3, the α_1 parameter is always found to be dominant. Therefore, in this section, to illustrate the role of the winding law in the determination of physics parameters, only the α_1 parameter will be considered. Figure 6 shows the effect of varying α_1 on the shape of the helical coil for an $M = 7$ torsatron. These changes of the winding law affect the physics properties of the configuration. Figure 7 shows the dependence on α_1 of the magnetic well, rotational transform, shear, and average radius of the last closed flux surface for the $M = 7$ configuration with a helical coil pitch $p_c = 1.3$. By choosing a positive value of α_1 , the average radius, edge rotational transform, and shear can be substantially increased over the values for $\alpha_1 = 0$. However, for positive α_1 , there is no longer a broad magnetic well, and even a magnetic hill across the whole radial extent can be generated for $\alpha_1 > 0.2$. To have deeper magnetic wells, it is necessary to choose negative values for α_1 . Therefore, the improvement of equilibrium and stability properties for these configurations cannot be achieved simultaneously by changing only the winding law parameters; and, as in the case of the cross section shaping, there is a trade-off between transform and well, which opens the possibility for configuration optimization. This optimization is discussed in detail in Section 3.

3 VACUUM MAGNETIC FIELD OPTIMIZATION OF LOW-ASPECT-RATIO TORSATRONS

As mentioned in the introduction, a major problem in optimizing the vacuum field configuration is finding an efficient method of dealing with the numerous degrees of freedom that characterize the coil winding law. The method of Cary and Hanson [5] offers a possible way of addressing this problem. The basic idea is to reconstruct the outer magnetic surfaces by reducing the stochasticity of the magnetic field lines. In this way, the size of the utilization volume and the edge transform can be increased. The method is based on minimizing the residue [9] of the periodic orbits, which is a measure of the island size at the corresponding magnetic surface. The stochasticity is reduced by decreasing the probability of island overlap through reducing the size of each magnetic island. The details of the method have been discussed elsewhere [5], so we mention only the constraints and parameters used for the minimization.

In the present studies, the optimization has focused on the equilibrium properties of low-aspect-ratio torsatron configurations. The goal is to increase the edge rotational transform and the utilization volume, but at the same time it is important to maintain or increase shear and magnetic well. This is achieved by doing a constrained minimization of the residues. The parameters that are kept constant are the axis rotational transform, $\iota(0)$, the axis magnetic well, through $V''(0)$, and the position of the magnetic axis, which is kept close to the center of the coil. For the lower- M configurations, the magnetic axis is slightly nonplanar. In these cases, the toroidal averaged position of the magnetic axis is maintained at the center of the coil. Parameters used for the minimization are the coil minor radius, \bar{a}_c (and hence the coil pitch), and the winding law parameters, α_n . In doing the minimization, it is sometimes necessary to relax the constraints and restrict the field of variation of the minimization parameters. Although this method provides a more systematic way of dealing with the numerous degrees of freedom of the coils, it is not a fully automatic process. The method does not lead to a unique solution for every M value. The resulting configuration depends on the initial configuration parameters, the values of the constraint parameters $\iota(0)$ and $V''(0)$, and other details of the minimization procedure. The solutions are also sensitive to the position of the magnetic axis with respect to the center of the coil (see Section 5).

The configurations resulting from this optimization calculation will be called Compact Torsatrons. The optimized configurations considered in this paper are designated by CTM, where M is the number of toroidal field periods. Four cases are considered, CT6, CT7, CT8, and CT9, which are torsatrons with 6 to 9 toroidal field periods. Figure 8 shows the vacuum magnetic field surfaces for these configurations. The four cases were selected on the basis of nearly constant rotational transform, close to 1, at the last closed flux surface. The main physics parameters for these four configurations are shown in Fig. 9, and the values obtained for the winding law parameters are listed in Table I. All four configurations have a plasma aspect ratio below 5, and the A_p for CT7 and CT6 is below 4. Some physics parameters of the Compact Torsatrons are similar to those of the ATF configuration [1]. Figure 10 shows the rotational transform and V' profiles for ATF and the CT6 configuration. To underline the similarity of these profiles, the values have been plotted vs the average radius normalized to the plasma minor radius. Although the two profiles are rather close, there are some differences between the two configurations. Apart from the aspect ratio, the main difference is in the variation of $\int d\ell/B$ over a magnetic

field period on a magnetic flux surface. This quantity is a measure of the Pfirsch-Schlüter currents. The CT configurations have larger values for the variation of $\int dl/B$ at the edge than the unoptimized configurations, and this value increases with decreasing M value.

Alternative optimization studies have been carried out using the parameters that control the shape of the torus winding cross section (e, a_1, a_2) and coefficients of higher harmonics in Eqs (1) and (2) as optimization parameters. When the ellipticity parameter is let free, the optimization moves toward a coil system with a highly elongated torus winding cross section. This strong ellipticity can be reduced by constraining the ellipticity parameter during the minimization. In either case, however, the coil system becomes very distorted, and it was not possible to raise the rotational transform at the edge above 1.0 or to reduce the aspect ratio below 5 for configurations with less than 8 toroidal field periods. Therefore, the only optimized configurations that we discuss further are the ones obtained using the winding law parameters.

4 MHD PROPERTIES OF THE COMPACT TORSATRON CONFIGURATIONS

The discussion of MHD properties of the CTs in this section assumes that magnetic surfaces exist for nonzero β values. The problem of the fragility of the magnetic surfaces is discussed in Section 5.

Equilibrium studies have been done with the 3-D equilibrium code VMEC [10]. This code uses a Fourier decomposition in the two angular coordinates to reduce the energy minimization problem to one of solving a large set of ordinary differential equations for the spectral coefficients. It is based on a Lagrangian formulation in which the magnetic surfaces are assumed to be nested. The equilibria obtained have been used to evaluate the 3-D Mercier stability criterion [11] for local instabilities. The form of the Mercier criterion is

$$D_M = D_S + D_W + D_I + D_G \geq 0 \quad (4)$$

where

$$\begin{aligned} D_S &= \frac{(\Psi''\Phi')^2}{r} \frac{s}{\epsilon^2 \pi^2} \\ D_W &= \frac{s}{\epsilon^2 \pi^2} \int \int g d\theta d\zeta \frac{B^2}{g^{**}} \frac{dp}{ds} \left(V'' - \frac{dp}{ds} \int \int \frac{g d\theta d\zeta}{B^2} \right) \\ D_I &= \frac{s}{\epsilon^2 \pi^2} \int \int g d\theta d\zeta \frac{B^2}{g^{**}} \left[\Psi'' I' - (\Psi'' \Phi') \int \int \frac{g (\vec{J} \cdot \vec{B}) d\theta d\zeta}{g^{**}} \right] \\ D_G &= \frac{s}{\epsilon^2 \pi^2} \left[\int \int \frac{g d\theta d\zeta (\vec{J} \cdot \vec{B})}{g^{**}} \right]^2 - \frac{s}{\epsilon^2 \pi^2} \left[\int \int \frac{g d\theta d\zeta (\vec{J} \cdot \vec{B})^2}{g^{**} B^2} \right] \left(\int \int \frac{g d\theta d\zeta B^2}{g^{**}} \right) \end{aligned}$$

Here, Φ and Ψ are the toroidal and poloidal magnetic flux functions, g is the jacobian, p is the pressure, I is the total toroidal current in a magnetic surface, and $g^{**} = |\vec{\nabla}s|^2$ is the corresponding metric element. The radial-like variable s is the toroidal flux normalized to 1 at the edge, and the primes indicate derivatives with respect to s . This form for the Mercier criterion is like the one given in Ref. 15. In this stability criterion, D_S gives the stabilizing contribution of the shear, D_W is the contribution of the magnetic well or hill, D_I (which is linear in the shear) gives the contribution of net currents, and D_G is the contribution of the geodesic curvature. Details of the numerical implementation and convergence studies are given in Ref. 16.

The Mercier stability studies have been complemented with stability studies for low mode numbers, $n = 1$ and 2 (here n is the toroidal mode number). These stability calculations are based on the stellarator expansion [7]. This approach to the stellarator MHD problem has been shown to be accurate for a large number of configurations [12,13]. However, for the low-aspect-ratio configurations studied in this paper, use of the stellarator expansion is questionable. For instance, in the case of the CT6 configuration, the magnetic axis shift as a function of the peak β , β_0 , is shown in Fig. 11. In this figure, results of the 3-D calculation are compared with results obtained using the stellarator expansion. These equilibrium calculations assume flux conservation and a pressure profile $p \sim \Phi^2$. The comparison clearly shows that the stellarator expansion overestimates the magnetic axis shift. Inaccuracy of the stellarator expansion is not surprising because the inverse aspect ratio, $\epsilon = 1/A_p$, for

the CT6 configuration is $\epsilon = 0.26$, which is no longer compatible with the ordering assumed for the expansion. Therefore, the stellarator expansion results for the Compact Torsatron configurations should be taken in a qualitative rather than a quantitative sense. The 3-D equilibrium calculations show that the equilibrium β limit increases with decreasing aspect ratio. Figure 12 compares the magnetic axis shift as a function of β_0 for the CT6 and CT8 configurations. The calculations are done for a fixed pressure profile, and the zero-net-current condition is used on each flux surface. The pressure profile used is $p \sim \Psi^2$, where Ψ is the poloidal magnetic flux. The figure shows that the magnetic axis shift at a given β is smaller for the CT6 configuration. To compare equilibrium properties for all these configurations, one can define the equilibrium β limit, β_c , as the value of β for which the magnetic axis shift is one-half the minor radius. The resulting β_c for the CT configurations is shown in Fig. 13. For comparison, the figure also includes the value obtained for an ATF-like configuration ($M = 12$), using the same pressure profile. These results indicate that β_c increases with decreasing M . This scaling is opposite to that usually attributed to stellarators. The reason is clear if the β limit scaling is assumed to be given by $\beta_c = \epsilon_a^2/A_p$. For a fixed-pitch sequence of configurations, the rotational transform is proportional to M and thus to the aspect ratio, $\epsilon_a \sim A_p$; therefore, $\beta_c \sim A_p \sim M$. In the present study, the CT sequence has constant rotational transform at the plasma edge, approximately equal to one; therefore, $\beta_c \sim 1/A_p \sim 1/M$. The ability to reconstruct the outer flux surfaces reverses the unfavorable scaling of equilibrium β for low-aspect-ratio stellarators.

The favorable stability properties of the low-aspect-ratio torsatron configurations are not lost in the equilibrium optimization process. Zero-net-current equilibria with pressure profiles $p \sim \Psi^2$ for the four CT configurations are stable to Mercier modes for practically the whole range of β values for which equilibrium exists. For low values of β ($\beta_0 < 3\%$) for the CT6 configuration, a small region with $D_M < 0$ appears near the magnetic axis. This problem can be eliminated by choosing flatter pressure profiles near the magnetic axis. D_M is positive over the whole plasma radius for higher β . Figure 14 shows the different contributions to the Mercier stability criterion for the CT6 configuration and for $\beta_0 = 11.7\%$. The dominant stabilizing term in the inner two-thirds of the minor radius is the magnetic well, D_W ; in the outer plasma region, the stabilization is the result of shear. This combination of well and shear is the basic stabilization mechanism for all the Compact Torsatron configurations. The minimum value of D_M moves from being near the magnetic axis at low β to near the plasma edge at higher β values. This is the result of broadening of the magnetic well with increasing β . The minimum value of D_M also increases with increasing β (Fig. 15), showing the β -self-stabilization effect [14], which is characteristic of the low-aspect-ratio torsatron configurations.

Stability calculations for low- n modes have been done with the FAR code [15,16], a fixed-boundary stability code based on the stellarator expansion approximation. Only stability with $n < 3$ has been considered. In general, it is found that the CT zero-net-current equilibria are stable and that the only way to induce instabilities is to use the vertical field to shift the plasma inward. These results are consistent with the Mercier stability calculations.

5 FRAGILITY OF THE MAGNETIC SURFACES FOR COMPACT TORSATRON CONFIGURATIONS

The reconstructed outer magnetic surfaces for the CT configurations are sensitive to magnetic perturbations. The main concern is with magnetic perturbations induced by non-zero β effects. Before studying the β effects, let us consider the case of a vacuum magnetic field subjected to an additional dipole magnetic field moment, which causes a shift of the magnetic axis. Four variations have been considered: the CT6 configuration (Fig. 16c) and the CT6 configuration with inward shifts of the magnetic axis of 2 cm (Fig. 16a) and 4 cm (Fig. 16b) and an outward shift of 2 cm (Fig. 16d). It is clear from the figure that the sensitivity of the outer surfaces to the axis shift is high. A 10% outward axis shift is enough to reduce the edge transform from 1 to 0.65 and to cause the destruction of 50% of the surfaces that have been reconstructed with the optimization method. This sensitivity is further underlined by combining the outward magnetic axis shift with a new optimization for the shifted configuration. Figure 17 shows a sequence of vacuum magnetic surfaces for configurations obtained in this way. It starts with the standard CT6 (Fig. 17a), and the other configurations are obtained by making successive 2-cm outward shifts of the magnetic axis; each shift is followed by an optimization using only the winding law parameters. The changes in the edge rotational transform and plasma size caused by the outward magnetic axis shift are shown in Fig. 18. They are contrasted with the values for the same parameters obtained after the optimization. In doing this sequential optimization, the parameter α_1 must be increased from 0.446 (Fig. 17a) to 0.795 (Fig. 17d). This implies major changes in the winding law of the helical coils, which cannot be realized in practice using compensating coils.

To see the effect of β on the magnetic surfaces, a 3-D equilibrium study of the CT configurations was done with the NEAR code [17]. As with VMEC, this 3-D equilibrium code solves the equilibrium problem by minimization of energy. However, the NEAR code uses an Eulerian formulation for finding an equilibrium because this allows the study of equilibria whose flux surface topology changes with pressure. A vacuum flux coordinate system is employed as the Eulerian frame of reference for the calculation. For the CT6 configuration, converged equilibria with good flux surfaces are obtained up to $\beta_0 \sim 5\%$ (Fig. 19). At higher β values, magnetic islands appear, and for $\beta_0 > 10\%$, no converged equilibrium solution was found. Similar results were obtained for the other CT configurations. The β effects are comparable to those induced by the shift of the vacuum magnetic axis.

Because an axisymmetric magnetic field, a dipole, can generate the nonaxisymmetric components that cause breaking of the magnetic surfaces, it is plausible that using axisymmetric fields could heal the magnetic surfaces. To test this hypothesis, the method discussed in Section 3 was reformulated to use the currents in an axisymmetric coil system as parameters for the equilibrium optimization. The VF coil system used for the $M = 6$ configuration is shown in Fig. 20. The system consists of four pairs of circular coils, positioned as indicated in the figure. The magnetic surfaces obtained after the optimization are shown in Fig. 21. The physics parameters obtained are close to those of the CT6 configuration. The currents required are large (on the order of the helical coil current) in the inner set of VF coils (VF1 in Fig. 20) but very weak in the outer VF coils. This shows that, with a properly designed VF coil system, the optimization method gives results very similar to those obtained by changing the winding law. This has two important consequences. First, the problem of accurately constructing a helical coil with the winding law of the type shown in

Eq. (3) is not overly demanding because the VF coil system can be used to correct for errors. Second, it gives a way of compensating for β effects on the magnetic surfaces in an experiment. This offers a potential solution to the problem of fragility of the magnetic surfaces for low-aspect-ratio configurations, but such a solution needs to be tested experimentally.

6 CONCLUSIONS

Low-aspect-ratio stellarator configurations with good flux surfaces can be realized by using torsatron windings. In particular, magnetic configurations that have utilization volumes with aspect ratios in the range of 3.5 to 5 can be realized by helical coil systems with aspect ratios of 2.5 to 3 and with 6 to 9 toroidal field periods.

These Compact Torsatrons are attractive stellarator configurations from the point of view of their equilibrium and stability properties and the relatively large plasma size that can be confined. The critical issue for these configurations is how well the magnetic surface breaking at nonzero β can be avoided by the use of an adequate VF coil system. This issue requires detailed experimental study in a device that is capable of accessing a high β regime.

REFERENCES

- [1] J. F. Lyon, B. A. Carreras, K. K. Chipley, M. J. Cole, J. H. Harris, et al., *Fusion Technology* **10**, 179 (1986).
- [2] M. Fujiwara, K. Matsuoka, K. Yamazaki, K. Nishimura, and T. Amano, in *Plasma Physics Laboratory Report PPLK-6, Vol. I*, p. 288 (1987).
- [3] J. Sheffield, R. A. Dory, S. M. Cohn, J. G. Delene, L. F. Parsly, et al., *Fusion Technology* **9**, 199 (1986).
- [4] J. F. Lyon, B. A. Carreras, S. L. Painter, J. S. Tolliver, and I. N. Sviatoslavsky, *Proceedings of the 14th European Conference on Controlled Fusion and Plasma Physics, 1987*, p. 353, Volume IID, European Physical Society, 1987.
- [5] R. Chodura, W. Dommaschk, F. Herrnegger, W. Lotz, J. Nuhrenberg, and A. Schluter, *IEEE Trans. Plasma Sci.* **PS-9**, 221 (1981).
- [6] J. R. Cary and J. D. Hanson, *Phys. Fluids* **29**, 2464 (1986).
- [7] J. M. Greene and J. L. Johnson, *Phys. Fluids* **4**, 875 (1961).
- [8] B. A. Carreras, H. R. Hicks, J. A. Holmes, V. E. Lynch, and G. H. Neilson, *Nucl. Fusion* **24**, 1347 (1984).
- [9] J. M. Greene, *J. of Math. Phys.* **20**, 1183 (1979).
- [10] S. P. Hirshman, W. van Rij, and P. Merkel, *Comput. Phys. Commun.* **43**, 163 (1986).
- [11] C. Mercier and H. Luc, *Lectures in Plasma Physics* (Commission of the European Communities, Luxemburg (1974), 1974).
- [12] B. A. Carreras, H. R. Hicks, J. A. Holmes, V. E. Lynch, L. Garcia, et al., *Phys. Fluids* **26**, 3569 (1983).
- [13] J. L. Johnson, *Computer Phys. Rep.* **4**, 37 (1986).
- [14] L. M. Kovrizhnykh and S. V. Shchepetov, *Soviet J. Plasma Phys.* **7**, 229 (1981).
- [15] L. A. Charlton, B. A. Carreras, H. R. Hicks, J. A. Holmes, and V. E. Lynch, *J. Comput. Phys.* **63**, 107 (1986).
- [16] V. E. Lynch, B. A. Carreras, L. A. Charlton, L. Garcia, T. C. Hender, H. R. Hicks, and J. A. Holmes, *J. Comput. Phys.* **66**, 441 (1986).
- [17] T. C. Hender, B. A. Carreras, L. Garcia, J. A. Rome, and V. E. Lynch, *J. Comput. Phys.* **60**, 76 (1985).

TABLE 1

WINDING LAW PARAMETERS

	$M = 9$	$M = 8$	$M = 7$	$M = 6$
α_1	0.27500	0.4695	0.35000	0.4460
α_2	-0.00435	-0.0804	-0.00789	-0.0079
α_3	0	0.0127	0.00450	0.0029
α_4	0	0	-0.00091	0.0009
α_c	0.3085	0.3400	0.3991	0.4000

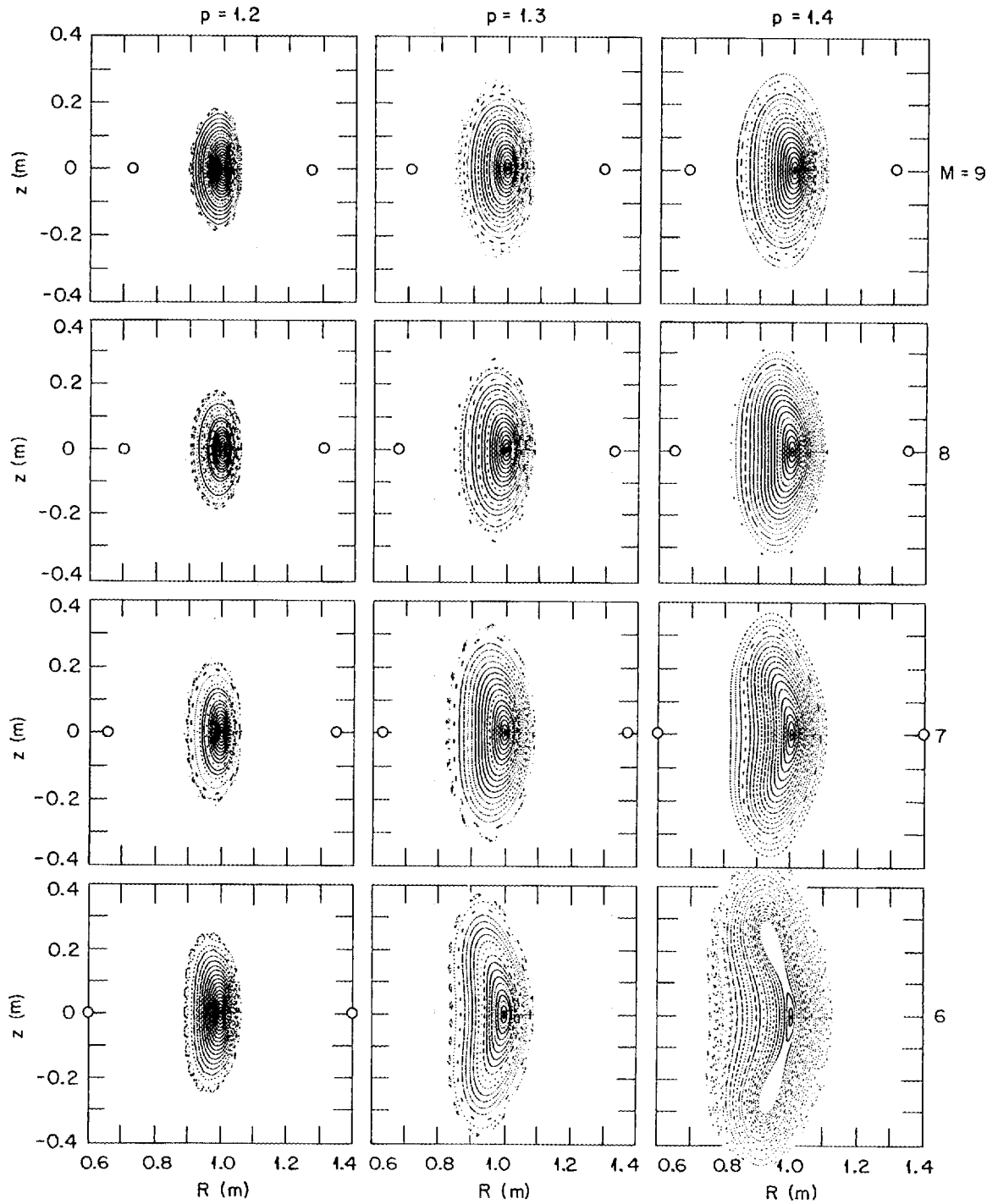


FIG. 1. Magnetic surfaces in the $\phi = 0^\circ$ plane for different torsatron configurations obtained by varying the number of field periods, M , and the pitch of the helical coil.

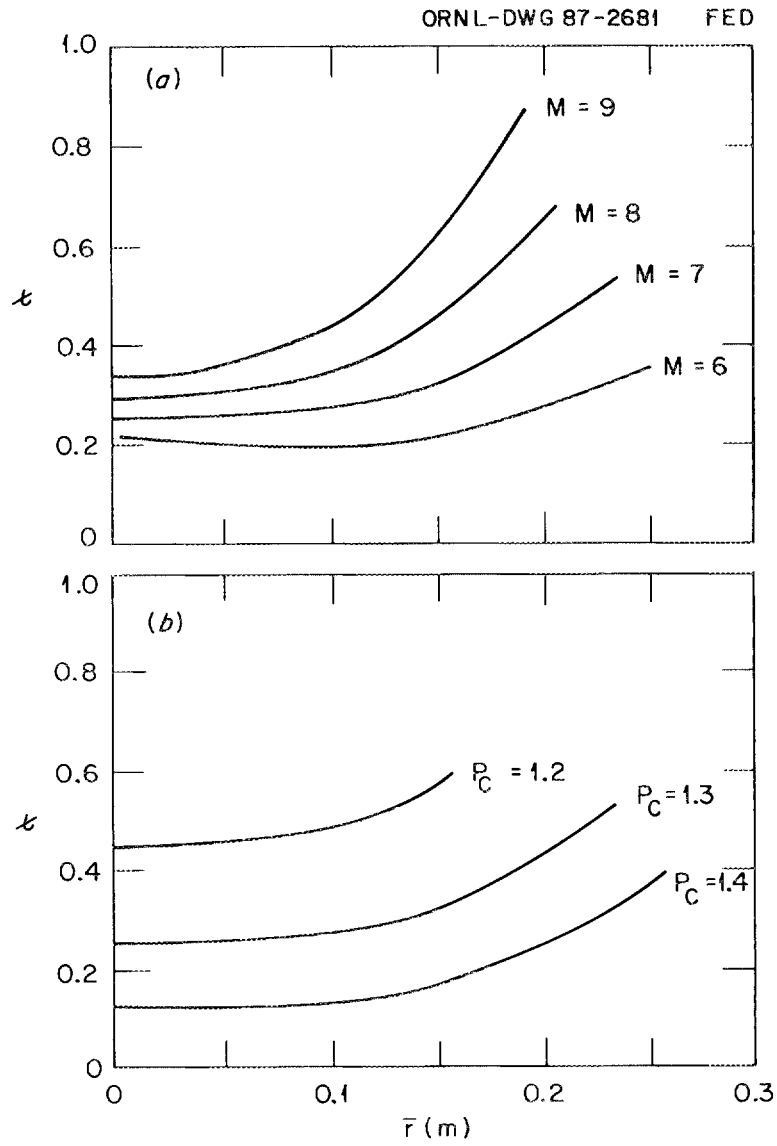


FIG. 2. Rotational transform profile for some configurations shown in Fig. 1: (a) with fixed pitch, $p_c = 1.3$, and (b) with fixed number of field periods, $M = 7$.

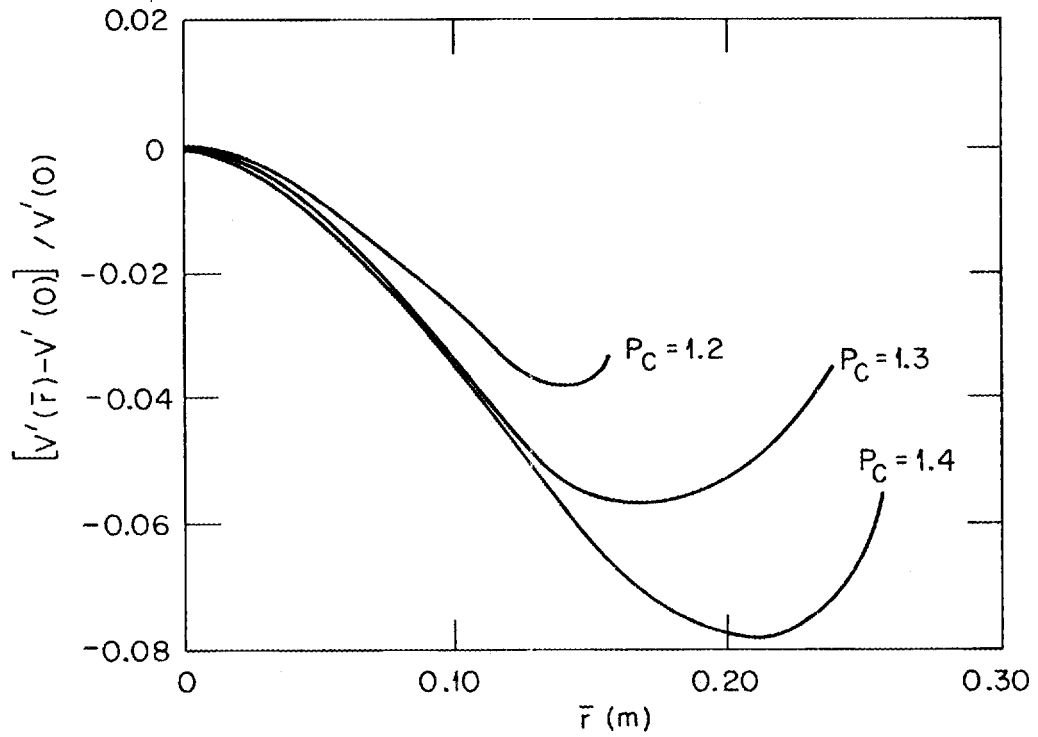


FIG. 3. Magnetic well profile for the configurations in Fig. 2b.

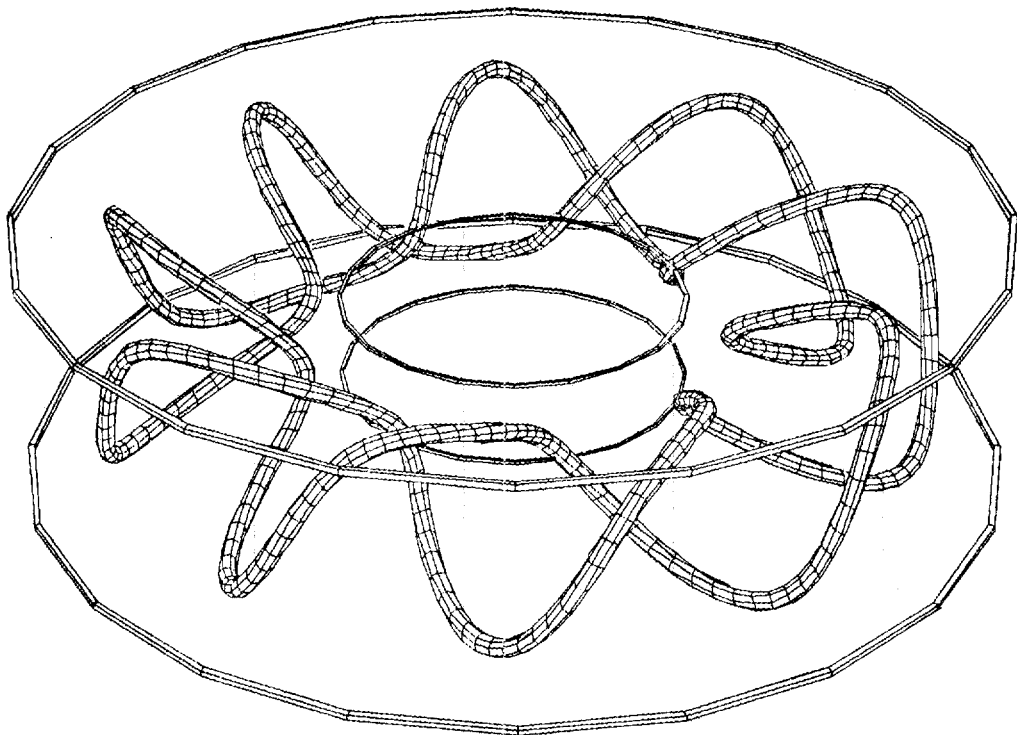


FIG. 4. Magnetic field coil system for an $M = 9$ torsatron configuration in which the helical coil has been wound on a triangular cross-section torus.

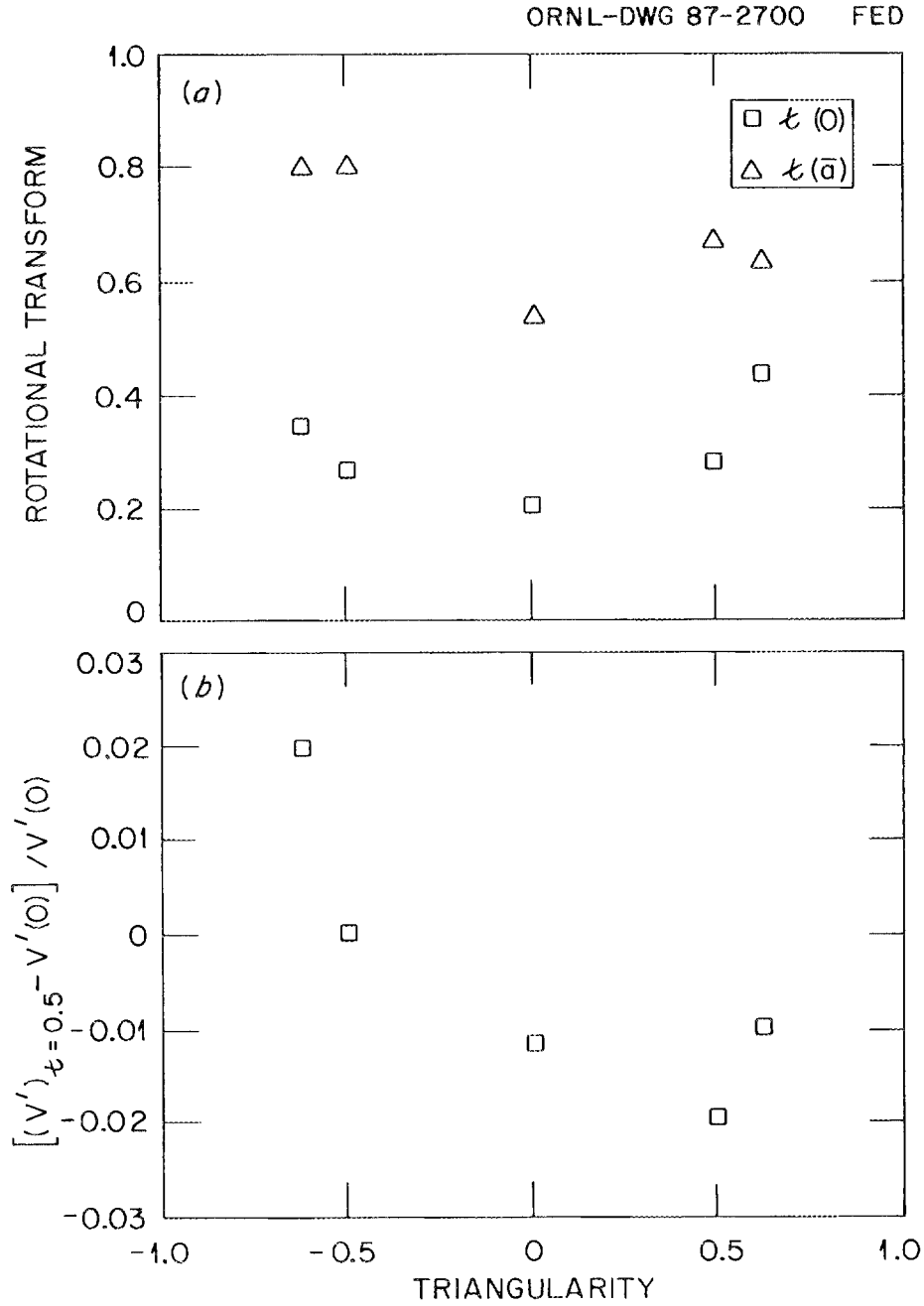


FIG. 5. Effect of triangularity on the physics parameters of an $M = 8$ torsatron configuration: (a) rotational transform at the axis, $t(0)$, and the edge, $t(\bar{a})$; and (b) magnetic well at the $\tau = 0.5$ surface.

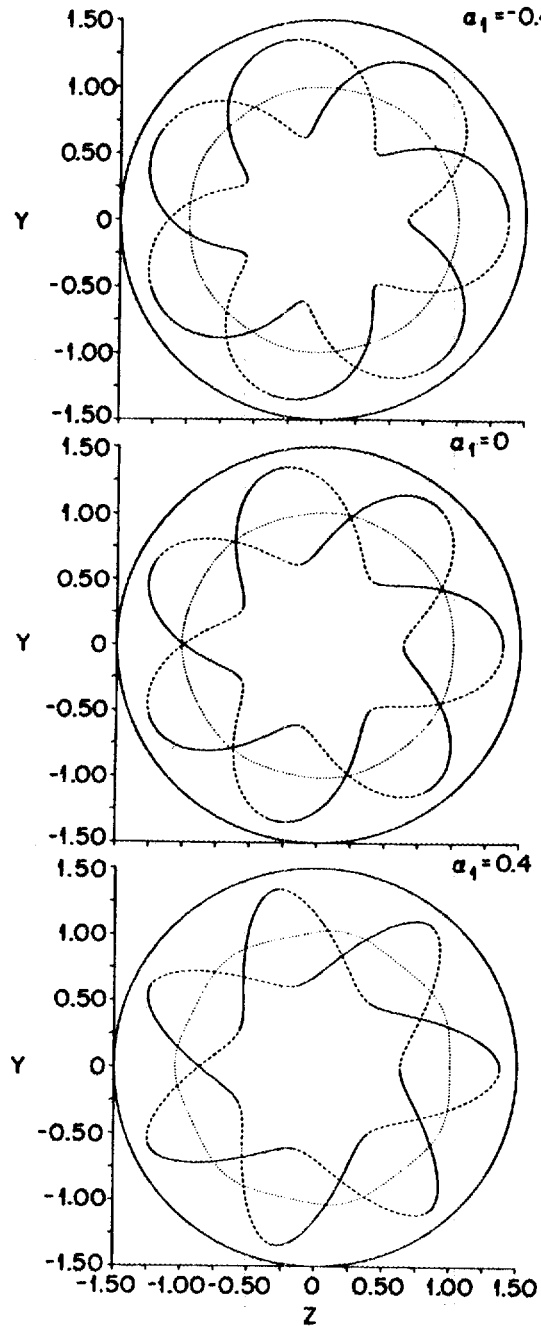


FIG. 6. Schematic top view of the magnetic field coil system for an $M = 7$ torsatron configuration with helical coil pitch $p_c = 1.3$ and different values of the winding law parameter α_1 .

ORNL-DWG 87-2697 FED

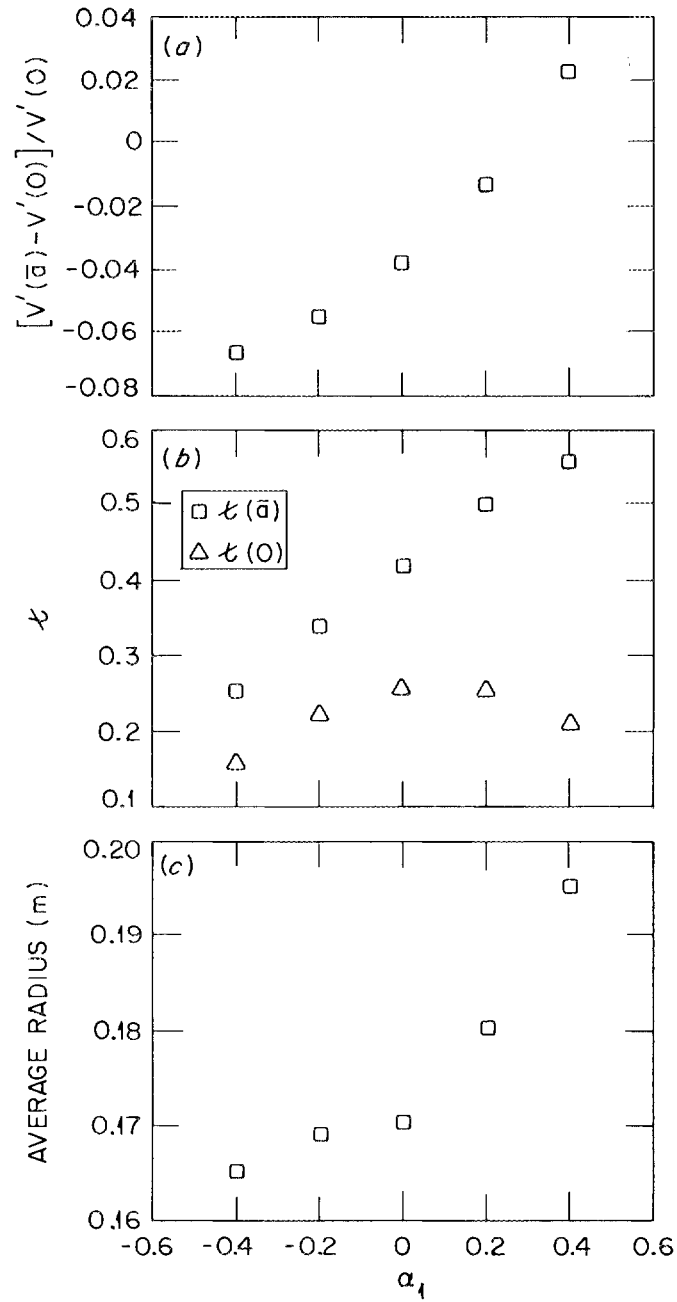


FIG. 7. Effect of the winding law parameter α_1 on the physics parameters of an $M = 7$ torsatron configuration with helical coil pitch $p_c = 1.3$: (a) magnetic well, (b) rotational transform at the magnetic axis and at the edge, and (c) average radius of the last closed flux surface.

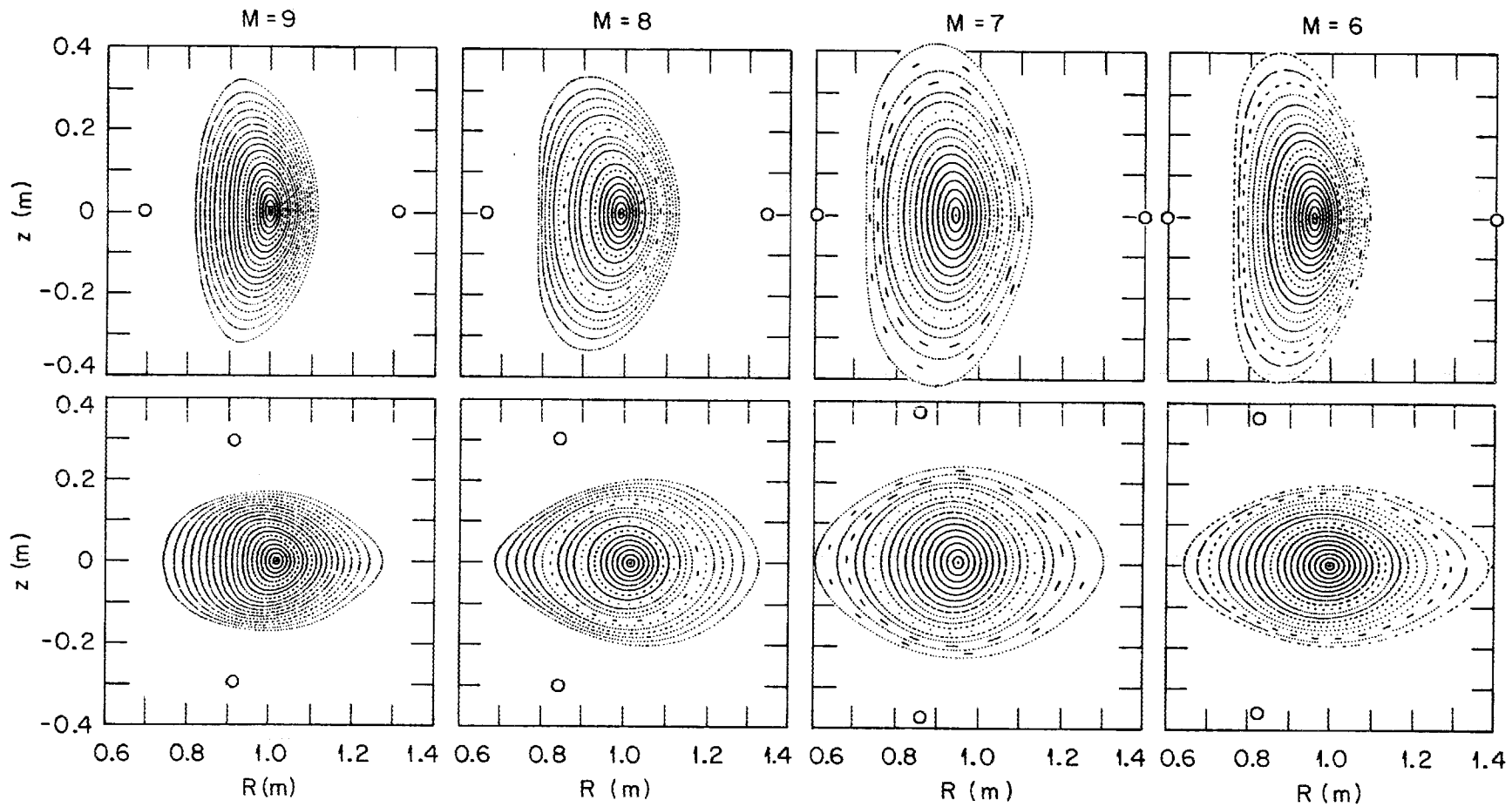


FIG. 8. Magnetic flux surfaces at the beginning and half-field period for the sequence of Compact Torsatron configurations studied in this paper.

ORNL-DWG 87-2698 FED

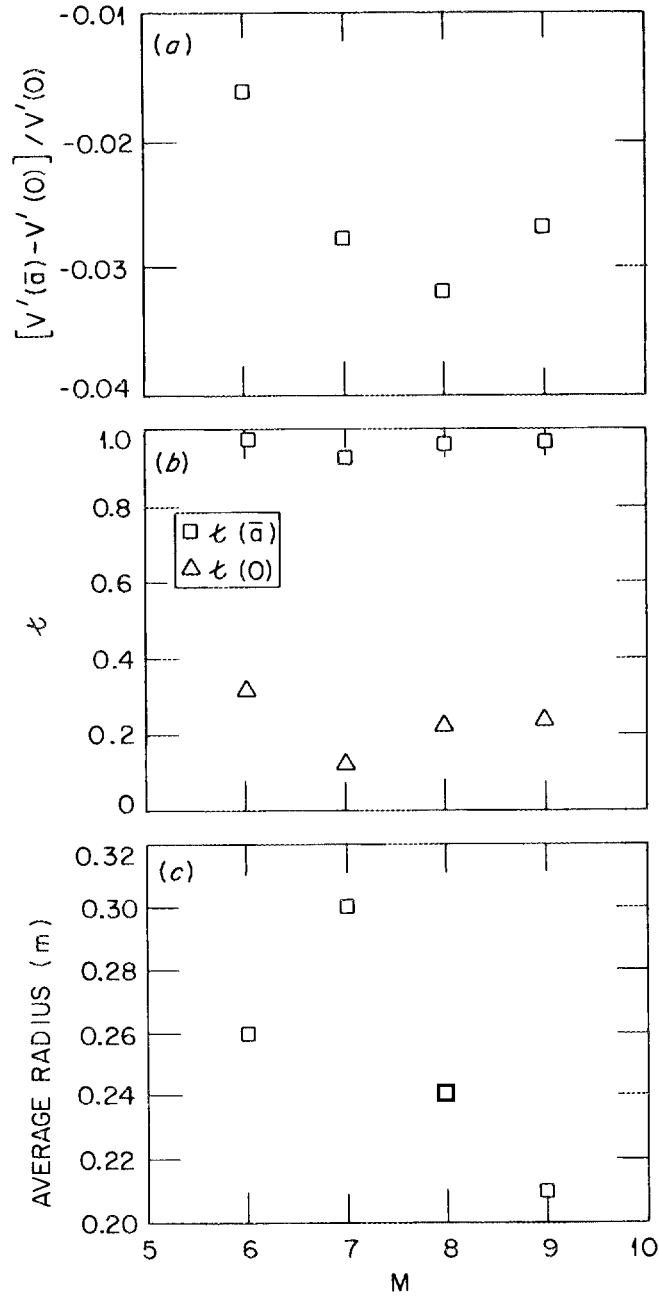


FIG. 9. Physics parameters for the sequence of configurations shown in Fig. 8: (a) magnetic well, (b) rotational transform, and (c) average radius of the last flux surface.

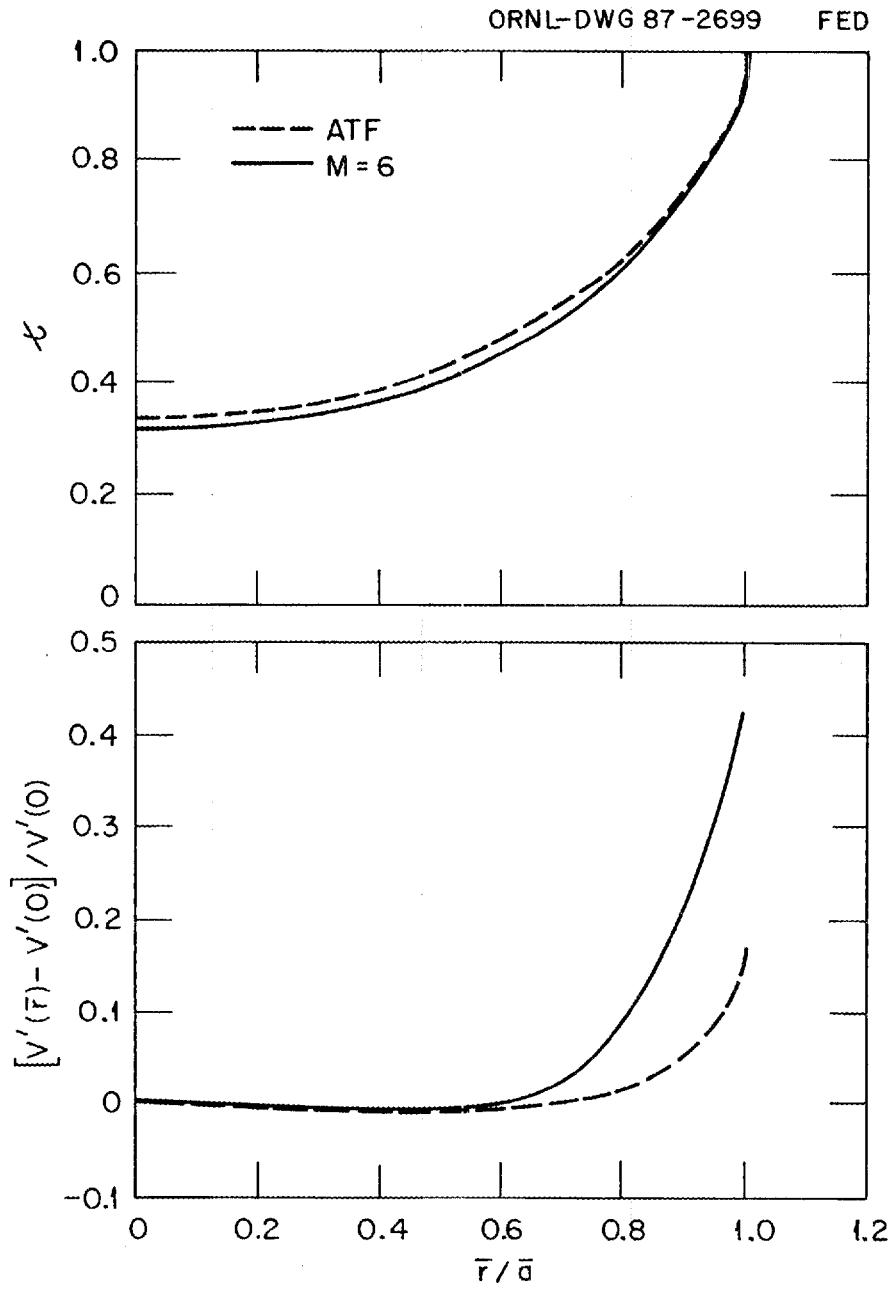


FIG. 10. Comparison of the rotational transform and magnetic well profiles for the CT6 and ATF configurations.

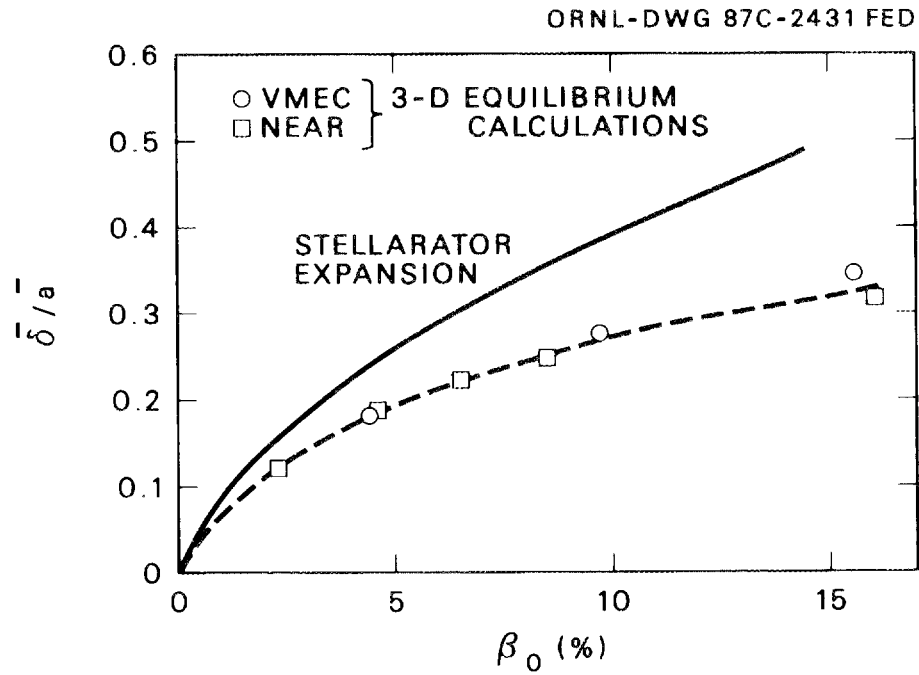


FIG. 11. Magnetic axis shift for the CT6 configuration obtained using the 3-D equilibrium codes VMEC and NEAR compared with the result from the stellarator expansion.

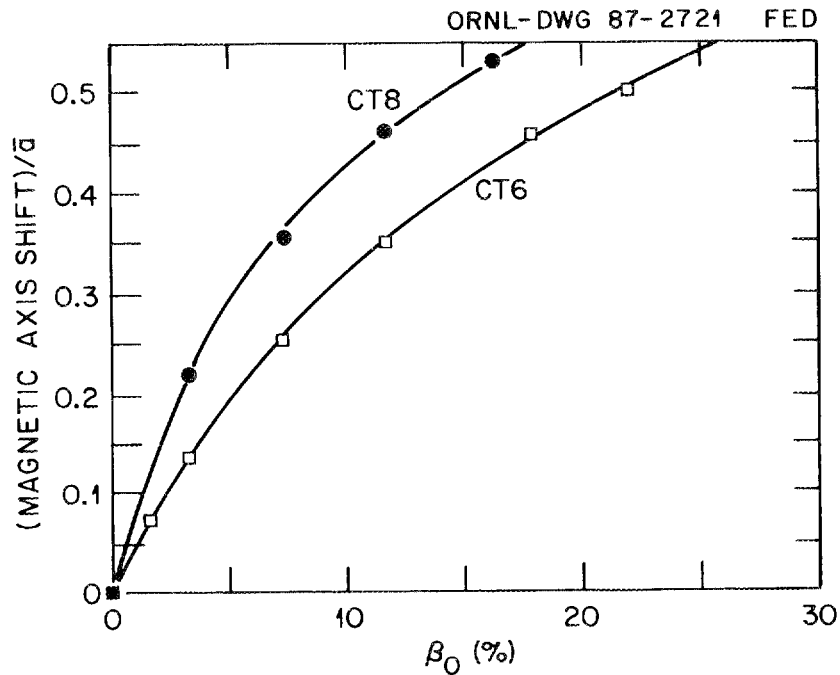


FIG. 12. Magnetic axis shift for the CT6 and CT8 configurations calculated with the VMEC equilibrium code.

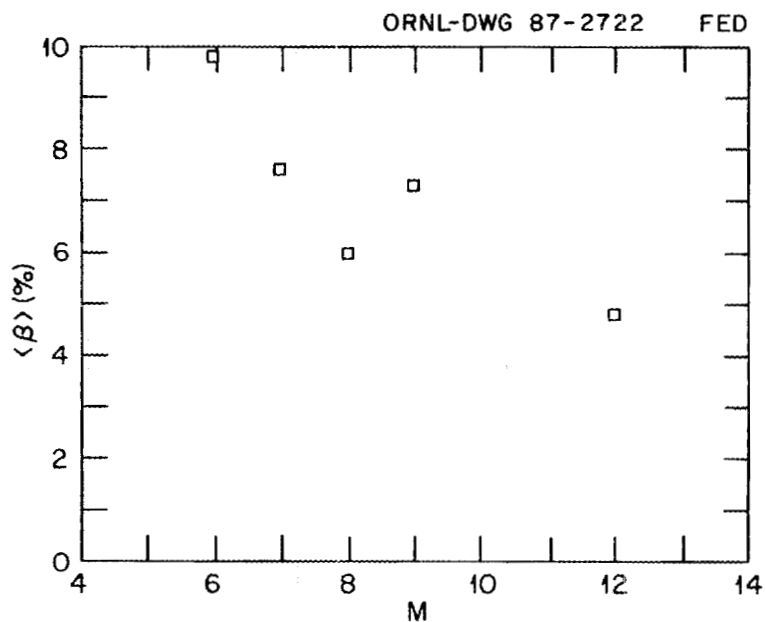


FIG. 13. Calculated equilibrium $\langle \beta \rangle$ limit for the sequence of Compact Toratron configurations.

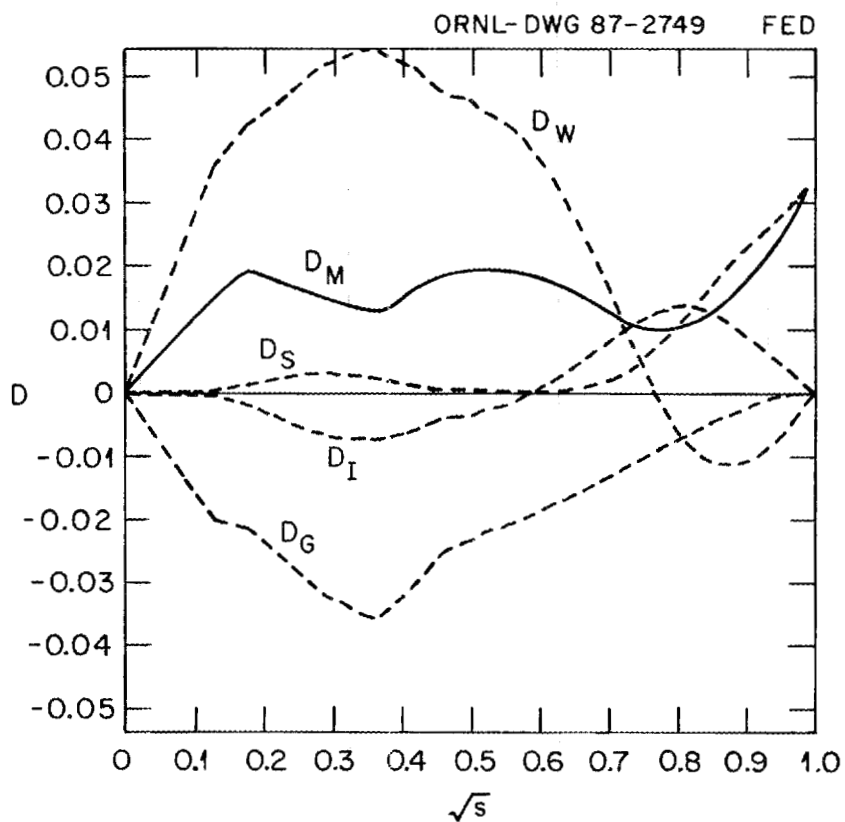


FIG. 14. Typical radial dependence of the contributions to the Mercier criterion, Eq. (4). The plotted values are for a $\beta_0 = 4\%$ equilibrium of the CT6 configuration.

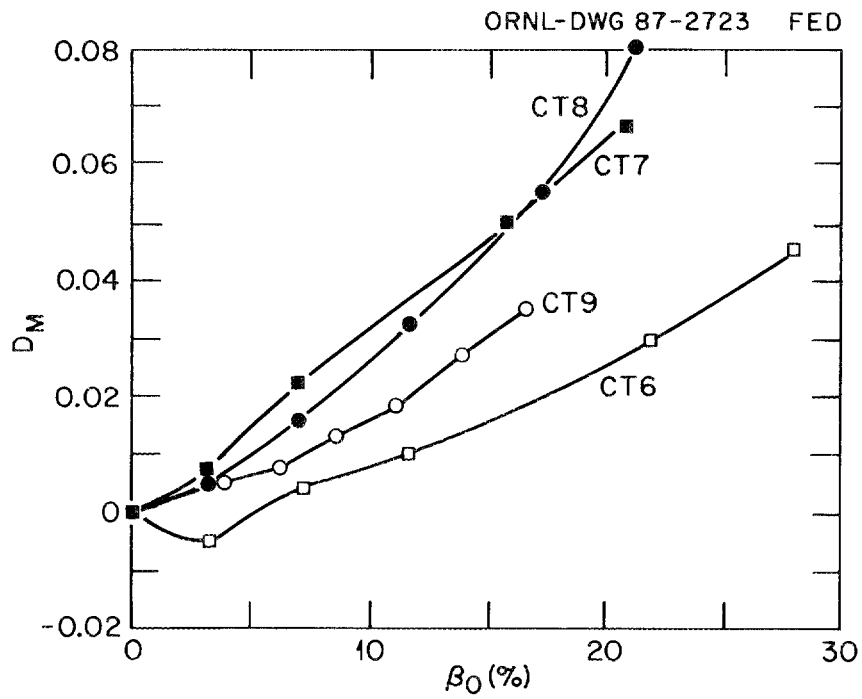


FIG. 15. Minimum value of D_M as a function of β_0 for the sequence of Compact Torsatron configurations.

ORNL-DWG 87-2433 FED

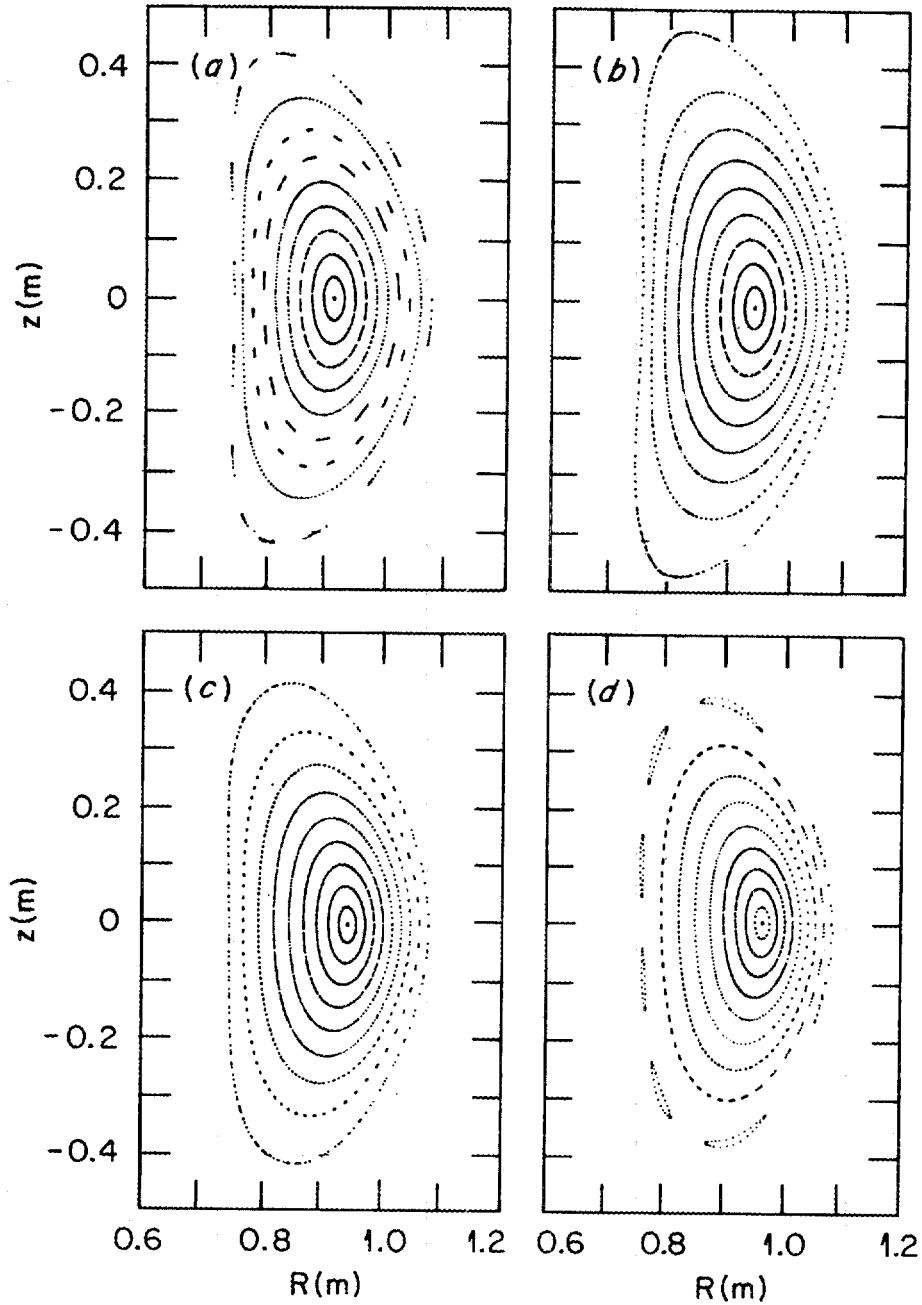


FIG. 16. Effect of a vacuum magnetic axis shift on the $\phi = 0^0$ magnetic surfaces of the CT6 configuration. The shifts are (a) $\Delta_v = -4$ cm, (b) $\Delta_v = -2$ cm, (c) $\Delta_v = 0$, and (d) $\Delta_v = 2$ cm.

ORNL-DWG 87-2399 FED

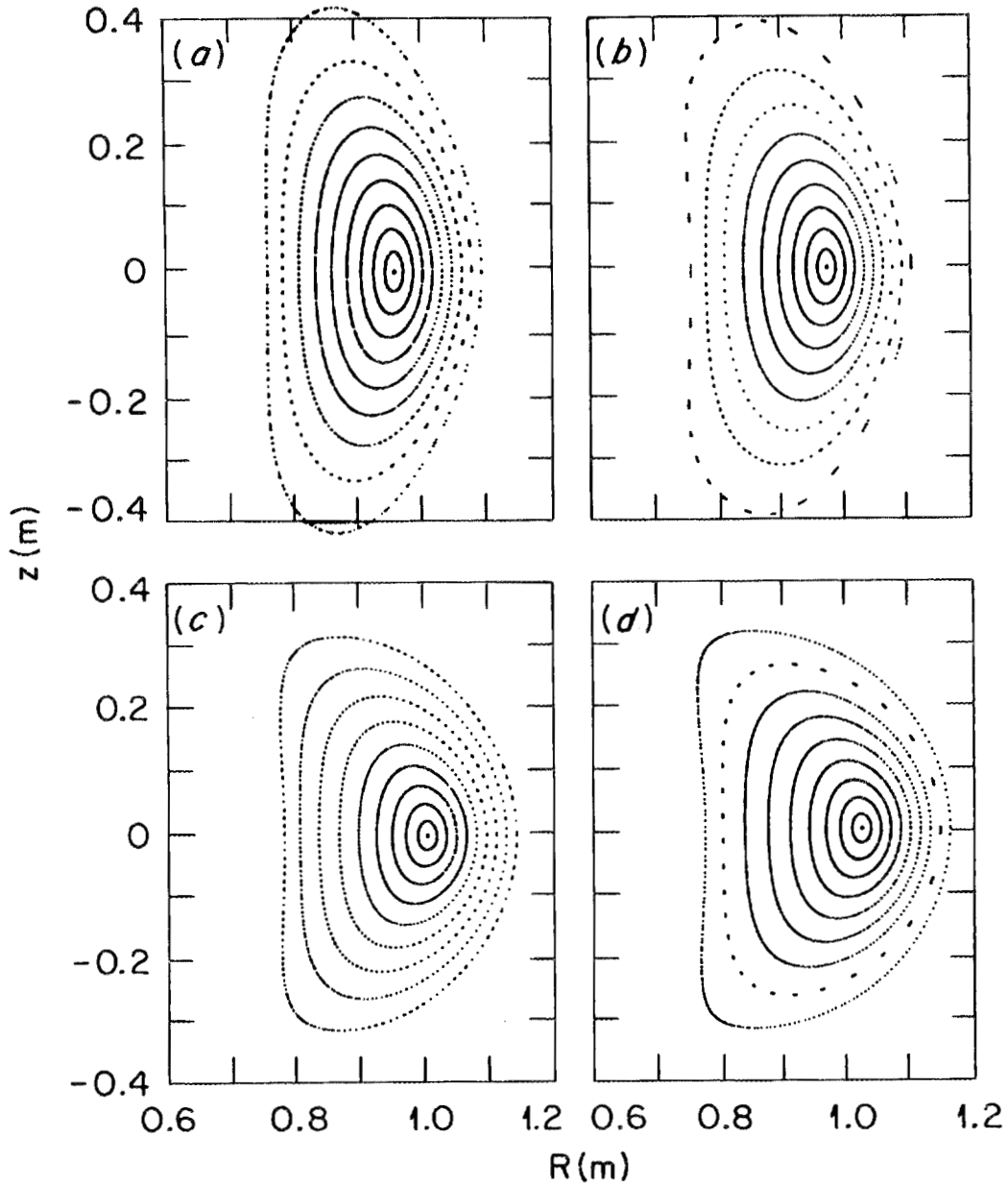


FIG. 17. Magnetic surfaces at the beginning of a field period for the CT6 configuration with an outer shift of the magnetic axis followed by optimization of the helical coil winding law. The axis shift and value of the α_1 parameter for the four cases are (a) $\Delta_v = 0$ and $\alpha_1 = 0.446$, (b) $\Delta_v = 2$ cm and $\alpha_1 = 0.540$, (c) $\Delta_v = 4$ cm and $\alpha_1 = 0.731$ and (d) $\Delta_v = 6$ cm and $\alpha_1 = 0.795$.

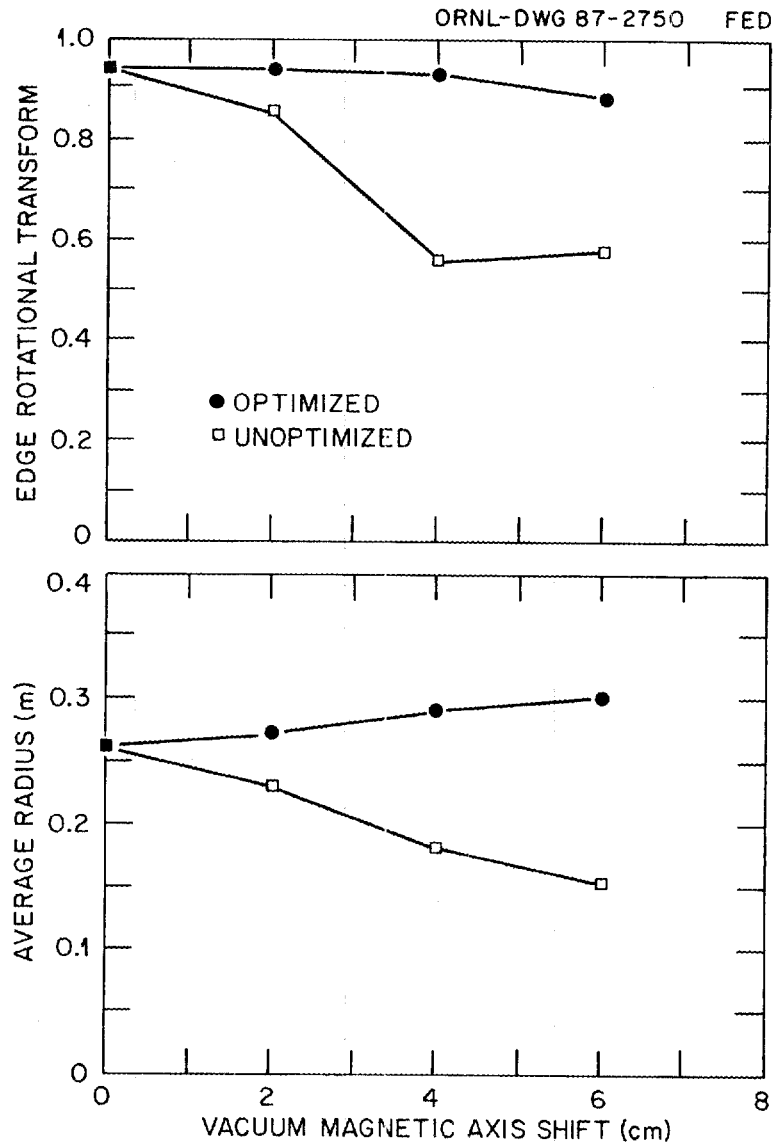


FIG. 18. Edge rotational transform and average radius of the last closed flux surface for the sequence of configurations in Fig. 17 compared with the corresponding configuration without optimization.

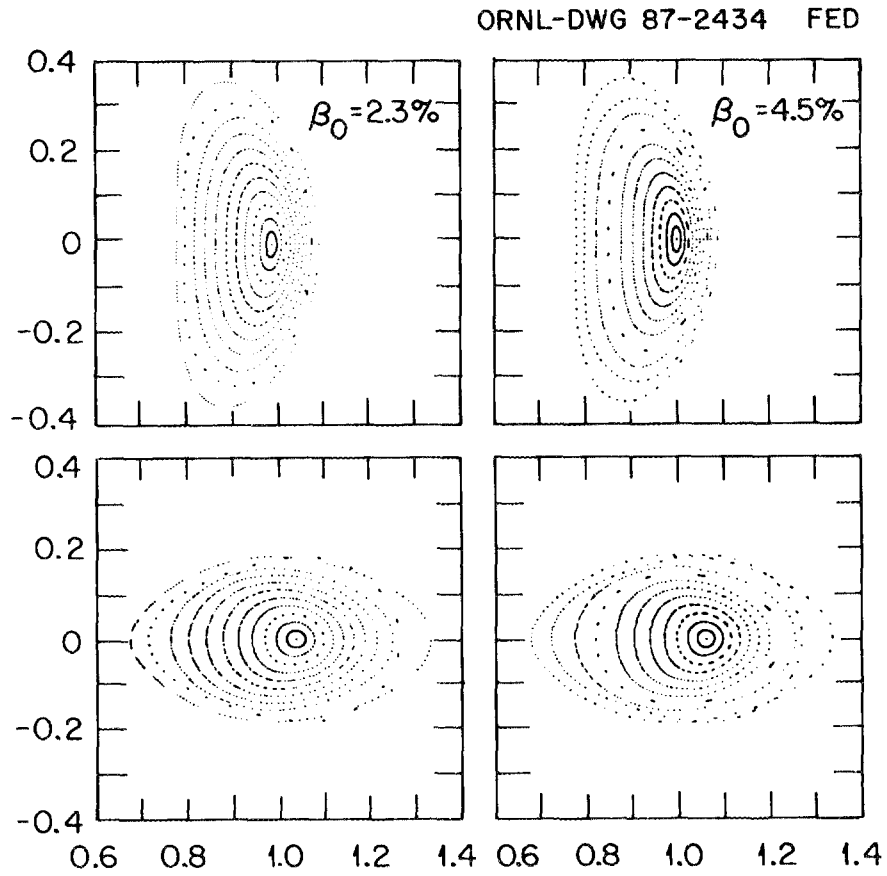


FIG. 19. Magnetic flux surfaces at the beginning and half-toroidal-field period for nonzero β equilibria for the CT6 configuration calculated using the 3-D equilibrium code NEAR.

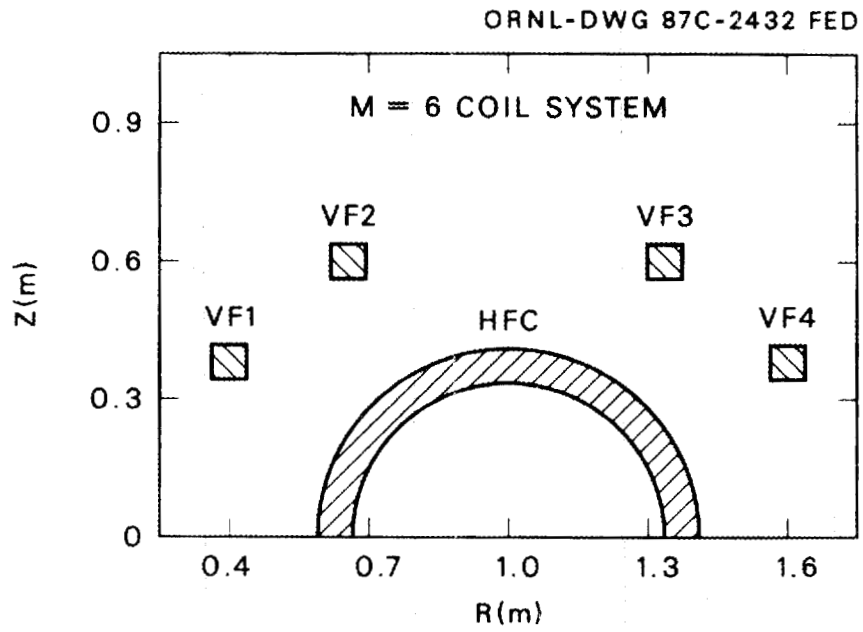


FIG. 20. Magnetic field coil system used for the optimization of flux surfaces for an $M = 6$ configuration.

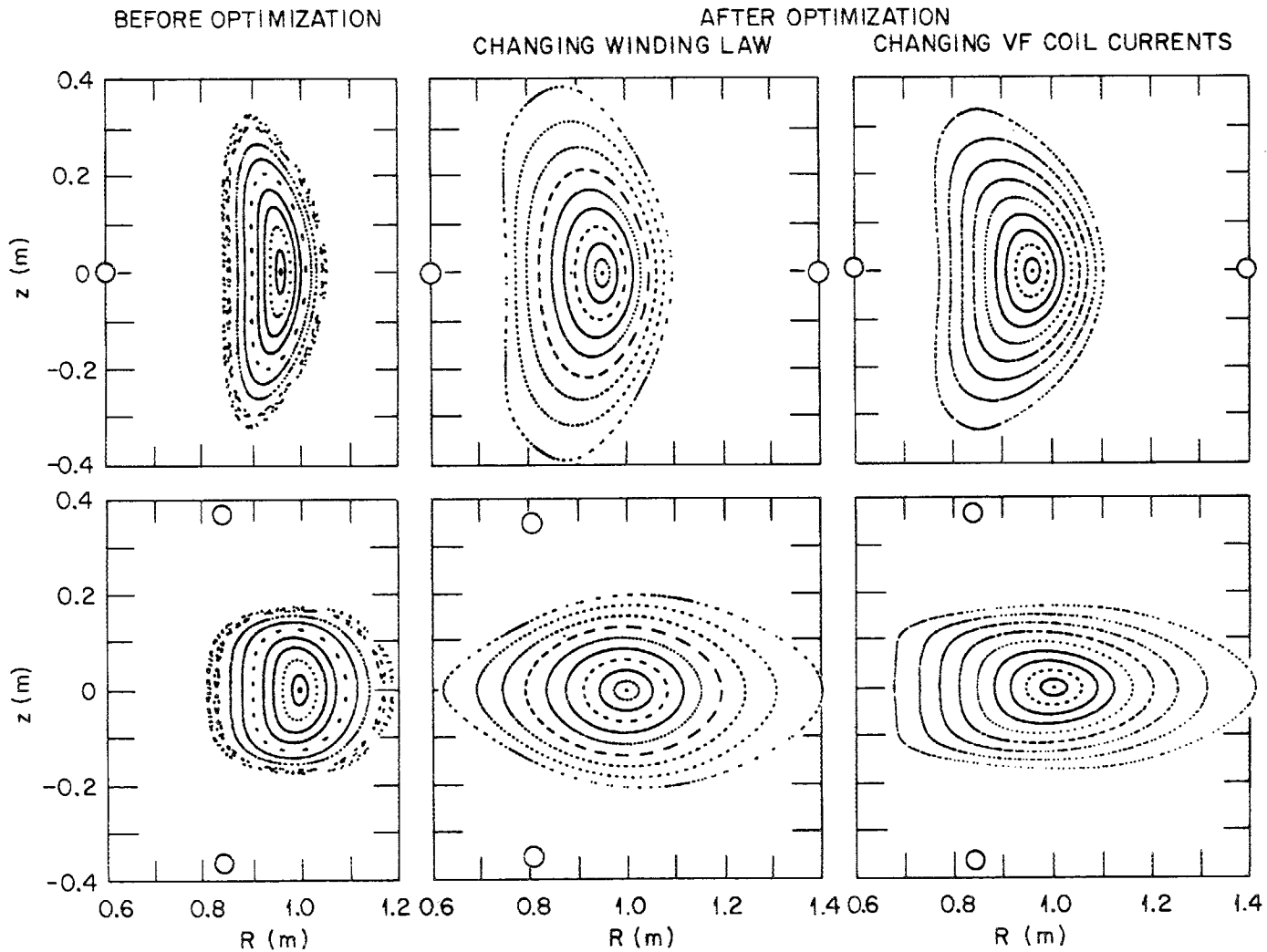


FIG. 21. Magnetic flux surfaces at the beginning and half-toroidal-field period before and after the optimization of flux surfaces.

INTERNAL DISTRIBUTION

- | | |
|----------------------|---|
| 1. L. A. Berry | 28-29. Laboratory Records Department |
| 2-10. B. A. Carreras | 30. Laboratory Records, ORNL-RC |
| 11-15. N. Dominguez | 31. Document Reference Section |
| 16. R. A. Dory | 32. Central Research Library |
| 17-21. V. E. Lynch | 33. Fusion Energy Division Library |
| 22-26. J. F. Lyon | 34-35. Fusion Energy Division Publications Office |
| 27. J. Sheffield | 36. ORNL Patent Office |

EXTERNAL DISTRIBUTION

37. J. R. Cary, University of Colorado, Boulder, CO 80304
38. J. D. Hanson, Auburn University, Auburn, AL 36848
39. A. P. Navarro, Asociacion EURATOM/CIEMAT, Av. Complutense, 28040 Madrid, Spain
40. L. Garcia Gonzalo, Dpto. Fisica Teorica, Facultad Ciencias Fisicas, Universidad Complutense, 28040 Madrid, Spain
41. P. H. Diamond, Institute for Fusion Studies, University of Texas, Austin, TX 78712
42. Office of the Assistant Manager for Energy Research and Development, U.S. Department of Energy, Oak Ridge Operations Office, P.O. Box E, Oak Ridge, TN 37831
43. J. D. Callen, Department of Nuclear Engineering, University of Wisconsin, Madison, WI 53706-1687
44. J. F. Clarke, Director, Office of Fusion Energy, Office of Energy Research, ER-50, Germantown, U.S. Department of Energy, Washington, DC 20545
45. R. W. Conn, Department of Chemical, Nuclear, and Thermal Engineering, University of California, Los Angeles, CA 90024
46. S. O. Dean, Fusion Power Associates, 2 Professional Drive, Suite 248, Gaithersburg, MD 20879
47. H. K. Forsen, Bechtel Group, Inc., Research Engineering, P.O. Box 3965, San Francisco, CA 94105
48. J. R. Gilleland, GA Technologies, Inc., Fusion and Advanced Technology, P.O. Box 81608, San Diego, CA 92138
49. R. W. Gould, Department of Applied Physics, California Institute of Technology, Pasadena, CA 91125
50. R. A. Gross, Plasma Research Laboratory, Columbia University, New York, NY 10027
51. D. M. Meade, Princeton Plasma Physics Laboratory, P.O. Box 451, Princeton, NJ 08544
52. M. Roberts, International Programs, Office of Fusion Energy, Office of Energy Research, ER-52 Germantown, U.S. Department of Energy, Washington, DC 20545

53. W. M. Stacey, School of Nuclear Engineering and Health Physics, Georgia Institute of Technology, Atlanta, GA 30332
54. D. Steiner, Nuclear Engineering Department, NES Building, Tibbetts Avenue, Rensselaer Polytechnic Institute, Troy, NY 12181
55. R. Varma, Physical Research Laboratory, Navrangpura, Ahmedabad 380009, India
56. Bibliothek, Max-Planck Institut fur Plasmaphysik, D-8046 Garching, Federal Republic of Germany
57. Bibliothek, Institut fur Plasmaphysik, KFA, Postfach 1913, D-5170 Julich, Federal Republic of Germany
58. Bibliotheque, Centre des Recherches en Physique des Plasmas, 21 Avenue des Bains, 1007 Lausanne, Switzerland
59. F. Prevot, CEN/Cadarache, Departement de Recherches sur la Fusion Controlee, 13108 Saint-Paul-lez-Durance Cedex, France
60. Documentation S.I.G.N., Departement de la Physique du Plasma et de la Fusion Controlee, Centre d'Etudes Nucleaires, B.P. 85, Centre du Tri, 38041 Grenoble Cedex, France
61. Library, Culham Laboratory, UKAEA, Abingdon, Oxfordshire, OX14 3DB, England
62. Library, FOM-Instituut voor Plasma-Fysica, Rijnhuizen, Edisonbaan 14, 3439 MN Nieuwegein, The Netherlands
63. Library, Institute of Plasma Physics, Nagoya University, Nagoya 464, Japan
64. Library, International Centre for Theoretical Physics, P.O. Box 586, I-34100 Trieste, Italy
65. Library, Laboratorio Gas Ionizzati, CP 56, I-00044 Frascati, Rome, Italy
66. Library, Plasma Physics Laboratory, Kyoto University, Gokasho, Uji, Kyoto, Japan
67. Plasma Research Laboratory, Australian National University, P.O. Box 4, Canberra, A.C.T. 2000, Australia
68. Thermonuclear Library, Japan Atomic Energy Research Institute, Tokai Establishment, Tokai-mura, Naka-gun, Ibaraki-ken, Japan
69. G. A. Eliseev, I. V. Kurchatov Institute of Atomic Energy, P.O. Box 3402, 123182 Moscow, U.S.S.R.
70. V. A. Glukhikh, Scientific-Research Institute of Electro-Physical Apparatus, 188631 Leningrad, U.S.S.R.
71. I. Shpigel, Institute of General Physics, U.S.S.R. Academy of Sciences, Ulitsa Vavilova 38, Moscow, U.S.S.R.
72. D. D. Ryutov, Institute of Nuclear Physics, Siberian Branch of the Academy of Sciences of the U.S.S.R., Sovetskaya St. 5, 630090 Novosibirsk, U.S.S.R.
73. V. T. Tolok, Kharkov Physical-Technical Institute, Academical St. 1, 310108 Kharkov, U.S.S.R.
74. Library, Academia Sinica, P.O. Box 3908, Beijing, China (PRC)

75. D. H. Crandall, Experimental Plasma Research Branch, Division of Development and Technology, Office of Fusion Energy, Office of Energy Research, ER-542 Germantown, U.S. Department of Energy, Washington, DC 20545
76. N. A. Davies, Office of the Associate Director, Office of Fusion Energy, Office of Energy Research, ER-51 Germantown, U.S. Department of Energy, Washington, DC 20545
77. D. B. Nelson, Director, Division of Applied Plasma Physics, Office of Fusion Energy, Office of Energy Research, ER-54 Germantown, U.S. Department of Energy, Washington, DC 20545
78. E. Oktay, Division of Confinement Systems, Office of Fusion Energy, Office of Energy Research, ER-55 Germantown, U.S. Department of Energy, Washington, DC 20545
79. W. Sadowski, Fusion Theory and Computer Services Branch, Division of Applied Plasma Physics, Office of Fusion Energy, Office of Energy Research, ER-541 Germantown, U.S. Department of Energy, Washington, DC 20545
80. P. M. Stone, Fusion Systems Design Branch, Division of Development and Technology, Office of Fusion Energy, Office of Energy Research, ER-532 Germantown, U.S. Department of Energy, Washington, DC 20545
81. J. M. Turner, International Programs, Office of Fusion Energy, Office of Energy Research, ER-522 Germantown, U.S. Department of Energy, Washington, DC 20545
82. R. E. Mickens, Atlanta University, Department of Physics, Atlanta, GA 30314
83. M. N. Rosenbluth, RLM 11.218, Institute for Fusion Studies, University of Texas, Austin, TX 78712
84. Duk-In Choi, Department of Physics, Korea Advanced Institute of Science and Technology, P.O. Box 150, Chong Ryang-Ri, Seoul, Korea
85. D. G. Swanson, Auburn University, Auburn, AL 36849
86. Theory Department Read File, c/o D. W. Ross, University of Texas, Institute for Fusion Studies, Austin, TX 78712
87. Theory Department Read File, c/o R. C. Davidson, Director, Plasma Fusion Center, NW 16-202, Massachusetts Institute of Technology, Cambridge, MA 02139
88. Theory Department Read File, c/o R. White, Princeton Plasma Physics Laboratory, P.O. Box 451, Princeton, NJ 08544
89. Theory Department Read File, c/o L. Kovrizhnykh, Lebedev Institute of Physics, Academy of Sciences, 53 Leninsky Prospect, 117924 Moscow, U.S.S.R.
90. Theory Department Read File, c/o B. B. Kadomtsev, I. V. Kurchatov Institute of Atomic Energy, P.O. Box 3402, 123182 Moscow, U.S.S.R.
91. Theory Department Read File, c/o T. Kamimura, Institute of Plasma Physics, Nagoya University, Nagoya 464, Japan
92. Theory Department Read File, c/o C. Mercier, Departement de Recherches sur la Fusion Controlee, B.P. No. 6, F-92260 Fontenay-aux-Roses (Seine), France
93. Theory Department Read File, c/o T. E. Stringer, JET Joint Undertaking, Culham Laboratory, Abingdon, Oxfordshire OX14 3DB, England
94. Theory Department Read File, c/o R. Briscoe, Culham Laboratory, Abingdon, Oxfordshire OX14 3DB, England

95. Theory Department Read File, c/o D. Biskamp, Max-Planck-Institut für Plasmaphysik, D-8046 Garching, Federal Republic of Germany
96. Theory Department Read File, c/o T. Takeda, Japan Atomic Energy Research Institute, Tokai Establishment, Tokai-mura, Naka-gun, Ibaraki-ken, Japan
97. Theory Department Read File, c/o V. Chan, GA Technologies, Inc., P.O. Box 85608, San Diego, CA 92138
98. Theory Department Read File, c/o L. D. Pearlstein, L-630, Lawrence Livermore National Laboratory, P.O. Box 5511, Livermore, CA 94550
99. Theory Department Read File, c/o R. Gerwin, CTR Division, Los Alamos National Laboratory, P.O. Box 1663, Los Alamos, NM 87545
- 100-215. Given distribution according to TID-4500, Magnetic Fusion Energy (Category Distribution UC-20 g, Theoretical Plasma Physics)